Supercontinuum generation in the picosecond regime

Arthur Zonnenberg

September 12, 2006

Contents

Abstract

In this report a 6 m NL-PM-750 fiber is pumped with 2 ps pulses from a mode-locked Ti-sapphire laser to generate a spectrally broad supercontinuum. Polarization, wavelength and power dependence of the generated supercotinua are measured. These results are then compared to two different models; one based on four wave mixing (FWM), the other based on solitons as the primary process for generating new spectral components. The FWM model is not adequate to describe the observed spectra. The soliton model uses a Raman-induced soliton self-frequency shift, couples solitons to dispersive waves and gives a better description of observed picosecond supercontinua.

1. Introduction and Motivation

A small, point-like illuminating source can be used to perform transmission and reflection measurements on a small object, such as a 50x50 μm sample. A supercontinuum is a spectrum with a broad spectral range. Supercontinua generated via nonlinear optical processes in photonic crystal fibers (PCFs) are bright - up to 3 orders of magnitude larger than an incandescent lamp [1] - and come at a small size (typically 1 to 10 μm). The goal is to generate a broadband spectrum at 750 and 1500 nm using a PCF. This fiber is specified to have two zero order dispersion wavelengths (one at 750 nm and one at 1260 nm) and is able to generate broadband spectra around those wavelengths using nonlinear processes. This bachelor research project has been performed with those objectives in mind, while gaining a better understanding of supercontinuum generation.

2. Theory

In this chapter a brief overview is given to cover the theory necessary to understand photonic crystal fibers (PCFs). The fiber design is explained in section 2.1. Linear optical properties and modal solutions are discussed in section 2.2. Fiber dispersion is so important it gets its own section 2.3, while nonlinear processes are introduced in section 2.4.

2.1. Fiber Design

Our index guiding PCF comprises a solid glass high index core embedded in an air-filled cladding structure where a number of air holes are arranged in a periodic pattern that runs along the length of the fiber, creating a hybrid air-silica material with a refractive index lower than that of the core.

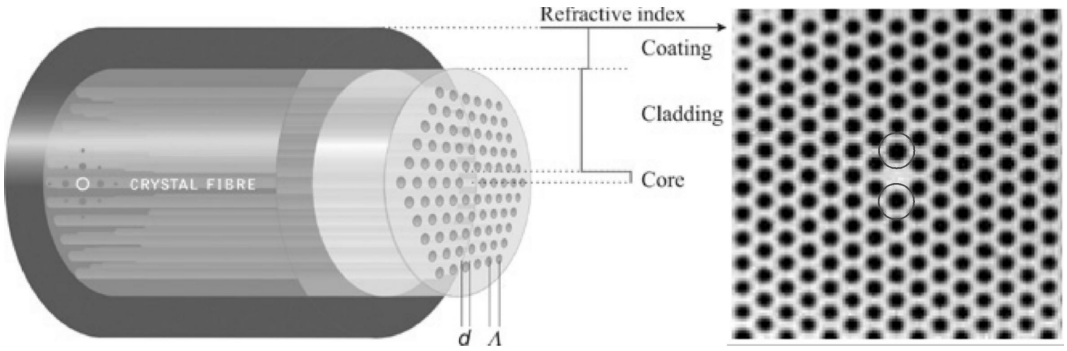

Figure 1: Left: Schematic of a triangular cladding single core PCF in which light is guided in a solid core embedded in a triangular lattice of air holes. The fiber structure is determined by the hole-size d, and the hole-pitch Λ. Right: SEM image of the cross-section of our fiber, taken from [2]. Two of the six air holes surrounding the core are slightly larger (circled) and cause the fiber to be birefringent.

In figure 1 (left) the structure of a typical PCF is shown. For our single-mode step-index PCF [4], the hole-pitch $\Lambda = 1.5\,\mu$m and the hole-size $d = 1.0\,\mu$m. The cross-section of our fiber is also shown (right). The core has a diameter of $1.8\,\mu$m and is surrounded by six air holes of which two are larger than the rest. This causes strong birefringence ($\Delta n > 3{\cdot}10^{-4}$) and makes the fiber polarization maintaining.

The relative hole diameter d/Λ compared to the relative wavelength λ/Λ of an optical field determines whether the fiber is single-mode or not [7].[1] There is a trade-off between entering the multimode region (losses due to higher order modes travelling slower), or entering the single-mode region (losses due to the mode propagating more through the cladding).

[1] If d/Λ becomes < 0.43, the fiber is single-mode for all wavelengths, also called endlessly single-mode [6]. The index difference between core and cladding becomes arbitrarily small as d/Λ goes to 0, but the single-mode does not disappear.

For our fiber the values of d and Λ ensure a good single-mode operation and put the cutoff wavelength for multi-mode operation $\leq 650\,\mathrm{nm}$. The cutoff wavelength of a single-mode fiber is the wavelength above which the fiber propagates only the fundamental mode. The fundamental mode can never be cut off [9].

2.2. Conventional Fiber Optics

Some insight into the properties of a PCF can be gained by treating the fiber as a conventional optical fiber. A conventional (step-index profile) fiber has a dielectric constant $\varepsilon(\overrightarrow{r},\omega)$ which is high within the core $r \leq a$ (with a the core radius) and low in the cladding $r > a$. Electromagnetic waves propagating through a fiber are described by the Helmholtz equation ([10], p. 501):

$$\nabla^2 E(\overrightarrow{r},\omega) + \varepsilon(\overrightarrow{r},\omega)\frac{\omega^2}{c^2}E(\overrightarrow{r},\omega) = 0, \tag{2.1}$$

The Helmholtz equation can be solved for the fiber geometry using the method of separation of variables. We introduce

$$E(\overrightarrow{r},\omega) = F(x,y)\exp(i\beta(\omega)z) \tag{2.2}$$

for a solution propagating in the positive z direction. For the part perpendicular to propagation this leads to

$$\frac{\partial^2 F}{\partial x^2} + \frac{\partial^2 F}{\partial y^2} + \left(\varepsilon(\overrightarrow{r},\omega)\frac{\omega^2}{c^2} - \beta^2(\omega)\right)F = 0 \tag{2.3}$$

where $r = \sqrt{x^2+y^2}$. The introduced β can be interpreted as a wavenumber of the solution, and gives the phase velocity in the z-direction. Equation 2.3 can be solved in cylindrical coordinates and yields Bessel functions inside the core and Neumann functions in the cladding. We will limit ourselves to a single propagation constant β, assuming that we are dealing with a single-mode fiber ([11], pp. 31-37; [12]).

2.3. Dispersion

Dispersion is the effect that the propagation constant β depends on ω. Dispersion plays an important role in pulse propagation because different spectral components of the pulse travel at different phase velocities given by ω/β. This is caused by two different contributions: material dispersion and waveguide dispersion.

Material dispersion reflects the fact that the refractive index of a material is frequency dependent, i.e. high-frequency (blue) components of an optical pulse travel slower than low-frequency (red) components of the same pulse. Each ω has its own modal distribution $F(x,y)$, part of which is in the core, and part of which is in the cladding. Waveguide dispersion is then the effect that due to the different modal distributions, the effective

index and therefore the propagation constant differ for different frequencies ω.

We define the derivatives of the propagation constant as:

$$\beta_m(\omega) = \frac{d^m \beta(\omega)}{d\omega^m} \qquad (m = 0, 1, 2, \dots) \tag{2.4}$$

The parameters $1/\beta_1$ and $1/\beta_2$ are known as the group velocity and the group velocity dispersion. An optical pulse, centered around the group frequency ω_0, moves at the group velocity $1/\beta_1$. The group velocity dispersion gives the spreading of the pulse in the temporal domain.

For wavelengths for which the fiber is said to exhibit normal dispersion ($\beta_2 > 0$), high-frequency (blue) components of an optical pulse travel slower than low-frequency (red) components of the same pulse. By contrast, the opposite occurs in the anomalous dispersion regime ($\beta_2 < 0$).

A zero-dispersion wavelength λ_D is defined as a wavelength for which $\beta_2 = 0$. Without group velocity dispersion, the shape of a pulse centered around $\omega_0 = 2\pi c/\lambda_D$ does not broaden or sharpen when propagating. In practice, bulk fused silica (glass) has one zero-dispersion wavelength at 1.31 μm ([11], p. 10). To get a second zero-dispersion wavelength, a waveguide contribution to dispersion is necessary. The waveguide contribution can be controlled by changing the hole-size d and the hole-pitch Λ. Figure 2 shows the dispersion of our PCF as a function of wavelength [2]. It has two zero-dispersion wavelengths at 750 and 1260 nm.

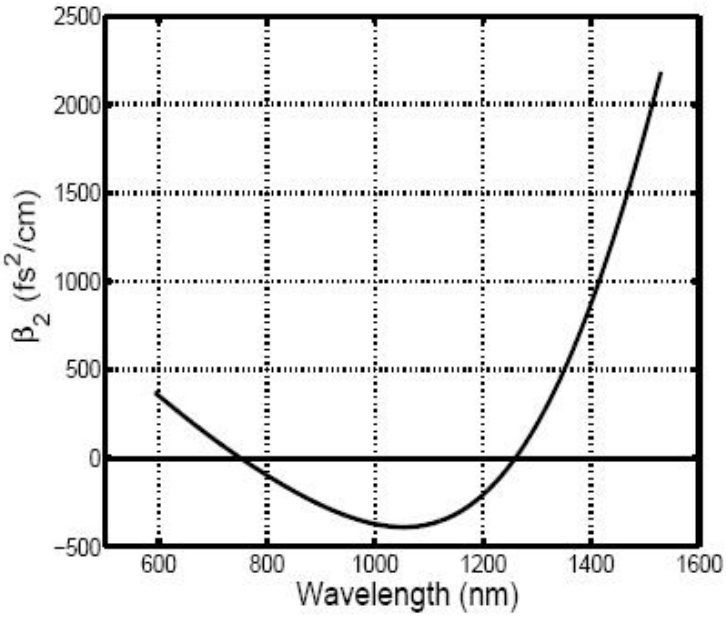

Figure 2: Dispersion of the NL-PM-750 PCF, taken from [2].

The measured [2] dispersion of our fiber (figure 2) can be approximated by a polynomial. This function can be found by fitting the dispersion curve to a polynomial of order n. We use a second order polynomial $\beta_2 = a+b\omega+c\omega^2$ and a least squares fitting method to determine the constants a, b and c. This gives the simplest mathematical form of β_2 that has two zero-dispersion wavelengths. To get a more accurate approximation of β_2 we also use a sixth order polynomial $\beta_2 = a + b\omega + c\omega^2 + d\omega^3 + e\omega^4 + f\omega^5 + g\omega^6$. The numerical data and coefficients that were fitted are given in appendix A.

2.4. Nonlinear Processes

In this section nonlinear processes relevant for supercontinuum generation are described. Self and cross phase modulation are described in section 2.4.1, followed by four wave mixing 2.4.2. Introducing the nonlinear change in refractive index leads to the nonlinear Schrödinger equation in section 2.4.3, under certain assumptions and approximations. When the contributions of self phase modulation and the nonlinear response to dispersion cancel each other, soliton solutions are found in section 2.4.4. Solitons in turn can be frequency shifted and coupled to dispersive waves.

2.4.1. Self Phase Modulation

Self phase modulation (SPM) is a nonlinear optical effect of light propagating through a dispersive medium. A high intensity pulse of light will induce a varying refractive index of the medium due to the optical Kerr effect. This variation in refractive index will produce a phase shift in the pulse, leading to a change in the frequency spectrum of the pulse.

Let us consider the propagation of the optical pulse

$$\widetilde{E}(z,t) = \widetilde{A}(z,t)\exp i(\omega_0 t - \beta_0 z) + c.c. \tag{2.5}$$

with $\beta_0 = \frac{n_0\omega_0}{c}$ through a medium characterized by a nonlinear refractive index of the sort

$$n(t) = n_0 + n_2 I(t), \tag{2.6}$$

where $I(t)$ is the intensity and n_2 is the nonlinear refractive index. Note that for the present we are assuming that the medium can respond essentially instantaneously to the pulse intensity. We also assume that the nonlinear medium is sufficiently short that no reshaping of the optical pulse can occur within the medium; the only effect of the medium is to change the refractive index n_0 to $n(t)$ in the instantaneous phase of the transmitted pulse:

$$\phi(t) = \omega_0 t - \frac{n(t)\omega_0 z}{c} \Rightarrow \Delta\phi(t) = -\frac{n_2\omega_0 z}{c} I(t) \tag{2.7}$$

where ω_0 is the (vacuum) center wavelength of the pulse, and z is the distance the pulse has propagated (in our case equal to the fiber length L). It is then intuitive to describe

the spectral content of the transmitted pulse by introducing the instantaneous frequency $\omega(t)$ of the pulse,

$$\omega(t) = \frac{d\phi(t)}{dt} = \omega_0 - \frac{n_2\omega_0 z}{c}\frac{dI(t)}{dt} \tag{2.8}$$

where the variation in frequency depends on the phase shift. This concept is well-defined and given by this equation whenever the amplitude $\widetilde{A}(t)$ varies slowly compared to an optical period. As an example we consider a pulse with intensity given by

$$I(t) = I_0 \exp\left(-\frac{t^2}{\tau^2}\right) \tag{2.9}$$

with τ the pulse width. The result is

$$\omega(t) = \omega_0 + \frac{n_2\omega_0 z}{c}\frac{2t}{\tau^2}I(t) \Rightarrow \Delta\omega(t) = \frac{2t}{\tau^2}\Delta\phi(t) \tag{2.10}$$

and plotted in figure 3.

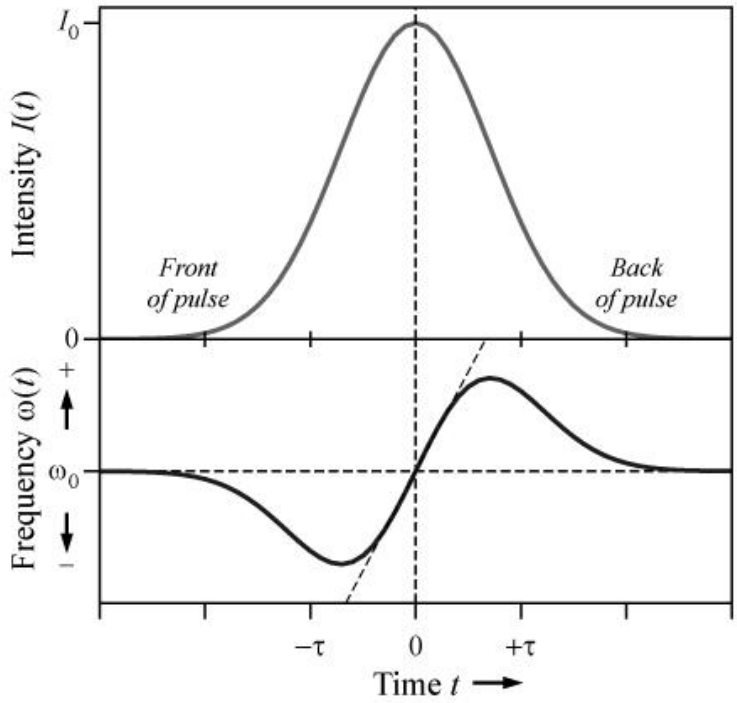

Figure 3: SPM for a Gaussian shaped pulse. The front of the pulse is shifted to lower frequencies, the back to higher frequencies. In the center the shift is approximately linear. Image taken from Wikipedia [5].

The phase shift $\Delta\phi(t)$ in equation 2.7 is set to 2π when the propagated distance z is equal to the nonlinear length L_{NL}, defined as

$$L_{NL} = (\gamma P_0)^{-1}, \tag{2.11}$$

where P_0 is the peak power ($P_0/A_{eff} = I_0$).[2] For our fiber $\gamma = 95\,(\mathrm{Wkm})^{-1}$. For a 2 ps pulse, with a 1 nJ pulse energy[3], the peak power P_0 is roughly estimated as 1 nJ/2 ps = 500 W. This gives a nonlinear length $(\gamma P_0)^{-1}$ of 2.1 cm, clearly smaller than our fiber length of $L = 6$ m.

The frequency shift in equation 2.10 can be written as

$$\Delta\omega(t) = \frac{n_2\omega_0 z}{c} I_0 \frac{2t}{\tau^2} \exp\left(-\frac{t^2}{\tau^2}\right) = \frac{L}{L_{NL}} \frac{2t}{\tau^2} \exp\left(-\frac{t^2}{\tau^2}\right) \tag{2.12}$$

This expression is maximal when $t = \pm\tau/\sqrt{2}$; for τ we take a pulse width of 2 ps, resulting in a frequency shift of $\Delta\omega = \pm 0.12{\cdot}10^{15}$. This corresponds to a spectral broadening of ± 45 nm for $\lambda_0 = 754$ nm, for our 6 m fiber.

Cross Phase Modulation

When two or more optical pulses propagate simultaneously through a fiber, they interact with each other in a similar manner through the fiber nonlinearity. If two carrier frequencies ω_1 and ω_2 are considered, the resulting nonlinear phase shift is given as ([11], p. 262)

$$\phi_{NL,j}(z) = -\frac{n_2\omega_0 z}{c}(|E_j|^2 + 2|E_{3-j}|^2) \tag{2.13}$$

where j = 1 or 2. The second term on the right-hand side is the XPM term and is twice as effective as SPM for the same intensity. Its origin can be traced back to the number of terms that contribute to the triple sum implied in the nonlinear polarization[4]

$$P_{NL}(r,t) = \varepsilon_0 \chi^{(3)} \vdots E(r,t)E(r,t)E(r,t) \tag{2.14}$$

When frequencies are non-degenerate the number of terms in the sum doubles for each frequency. The result of the XPM nonlinear phase shift is an asymmetric spectral broadening.

2.4.2. Four Wave Mixing

Four Wave Mixing (FWM) is a third order parametric process that can be quite efficient for generating new waves. We consider four optical waves oscillating at frequencies $\omega_1, \omega_2, \omega_3$ and ω_4 which are linearly polarized along the same axis x. For example, ([11], pp. 389-392; [14], pp. 245-252), 3 photons of the same frequency can produce a 4th photon (3rd harmonic generation), or 2 photons of the same frequency can produce a stokes and an anti-stokes photon (four wave mixing). Energy conservation for four wave mixing leads to:

$$\omega_1 + \omega_2 = \omega_3 + \omega_4 \tag{2.15}$$

[2] The effective core area of $A_{eff} = 2\mu\mathrm{m}^2$ is already incorporated in γ.
[3] 1 nJ corresponding to 80 mW average coupled power (see section 3.2) at a repetition rate of 80 MHz
[4] $D = \varepsilon_0 E + P, P = P_L + P_{NL}$

The phase-matching condition for this process to occur is

$$\Delta\beta = \beta(\omega_1) + \beta(\omega_2) - \beta(\omega_3) - \beta(\omega_4) = 0 \tag{2.16}$$

It is relatively easy to satisfy $\Delta\beta = 0$ in the case that $\omega_1 = \omega_2$. This partially degenerate case is the most relevant here: a strong pump wave at ω_1 creates two sidebands located symmetrically at frequencies ω_3 and ω_4 with a frequency shift

$$\Omega_S = \omega_1 - \omega_3 = \omega_4 - \omega_1 \tag{2.17}$$

the low-frequency sideband at ω_3 is also known as the Stokes or signal band, while the high-frequency sideband at ω_4 is also known as the anti-Stokes or idler band.

If we rewrite equation 2.16 in terms of pump, source and idler we get

$$\Delta\beta = 2\beta(\omega_p) - \beta(\omega_s) - \beta(\omega_i) = 0 \tag{2.18}$$

where the subscripts p, s and i stand for pump, signal and idler respectively. This equation is our phase-matching condition and is used to predict the frequencies of the sidebands. First, we approximate β_2 using the approximating polynomials from section 2.3. Second, we integrate $\beta_2(\omega)$ twice with respect to ω to get the following function:

$$\beta(\omega) + B\omega + C \tag{2.19}$$

where B and C are arbitrary integration constants. It is not difficult to show (with the help of equation 2.15) that the integration constants do not matter for the phase-matching condition; B and C can therefore safely be set to zero. Physically, this corresponds to the fact that the nonlinear interaction is always phase-matched if the dispersion is linear. Finally, we numerically solve equation 2.18.

The calculated frequencies ω_s and ω_i are given in figures 4 and 5. Figure 4 shows the solution for a 2nd order polynomial, while figure 5 shows the solution for a more realistic 6th order polynomial. A polynomial of degree n has n zeroes, and in general has complex (and/or real) solutions. The color of the dots in the figures indicate whether the solution is real[5] (red) or complex (yellow). Only the red dots (real solutions) represent physical frequencies. The most outlying curve represents wavelengths that directly satisfy 2.18. We then changed the right-hand side of equation to 0.05, 0.1, 0.15 and 0.2, being proportional to values of γP_0 ([11], pp. 394-397). This value includes the change in refractive index of the material at high optical intensities. These curves will be compared to experimental data in section 5.1.

[5]The imaginary part of the real solutions is very close to 0 (¡ 0.001 nm) for both simulations.

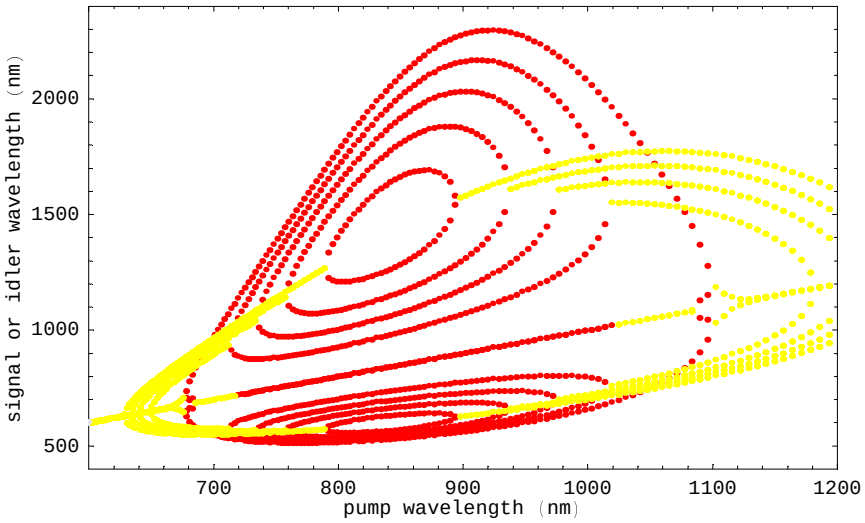

Figure 4: The phase-matching condition generates a set of solutions for values of the right-hand side of equation 2.18 set to 0, 0.05, 0.10, 0.15 and 0.20 (from out to in for the red curves). β_2 has been approximated by a 2nd order polynomial. Note that the outmost lying real curve (red) is bounded by pump wavelengths of ∼680 and ∼1100 nm, which are zeroes of the 2nd order polynomial fit.

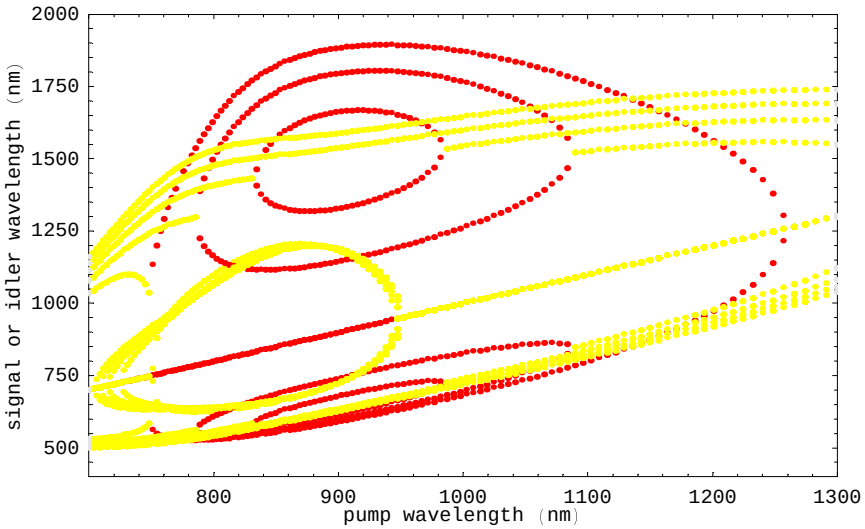

Figure 5: The phase-matching condition generates a set of solutions for values of the right-hand side of equation 2.18 set to 0, 0.05 and 0.10 (from out to in for the red curves). β_2 has been approximated by a 6th order polynomial. Due to the better fit, the outmost lying real curve (red) is better bounded by pump wavelengths of ∼750 and ∼1260 nm, which are the zero order dispersion wavelengths.

2.4.3. The Nonlinear Schrödinger Equation

The nonlinear optical response of a fiber can be treated as a small perturbation. Our fiber designed to have birefringence, and because of this it is polarization-maintaining. Therefore, the optical field is assumed to maintain its polarization along the fiber length so that a scalar approach is valid. Furthermore, the optical field is assumed to be quasi-monochromatic, i.e., the pulse spectrum, centered at ω_0, is assumed to have a spectral width $\Delta\omega$ such that $\Delta\omega/\omega_0 \ll 1$. Since $\omega_0 \sim 10^{15}$ s^{-1} for visible light, this is valid for pulses as short as 10 fs ($\Delta\omega/\omega_0 = 0.05$ for $\lambda_0 = 940$ nm). This assumption is equivalent to saying that the amplitude of the pulse envelope is slowly varying due to the changing of phase velocities.

We neglect the Raman response of the medium ([11], p. 40; [14], p. 375). In general, both electrons and nuclei respond to the optical field in a nonlinear manner. The nuclear response is inherently slower compared with the electronic response. For silica fibers the vibrational or Raman response occurs over a time scale of 60-70 fs. This is slow compared to the time scale of the electron response which is assumed to be instantaneous (i.e. response time = 0).

Using the above assumptions and approximations, equation 2.1 can be written as an equation in the propagation direction for a pulse with an amplitude $A(z, \omega)$. This is done by assuming a solution of the form

$$E(\overrightarrow{r}, \omega) = A(z, \omega)F(x, y)\exp(i\beta(\omega)z) \tag{2.20}$$

instead of equation 2.2 and by introducing the nonlinear response into $\varepsilon(\overrightarrow{r}, \omega)$. In addition, higher order dispersion terms (β_3, β_4, etc.) are neglected and we work in the frame of reference of an observer travelling with the group velocity ($1/\beta_1$). The resulting equation is known as the nonlinear Schrödinger equation (NLSE) ([11], p. 44; [14], p. 280):

$$\frac{\partial A}{\partial z} + \tfrac{1}{2}i\beta_2\frac{\partial^2 A}{\partial t^2} = i\gamma|A|^2A, \tag{2.21}$$

with the nonlinear coefficient γ defined as:

$$\gamma = \frac{n_2\omega_0}{cA_{eff}} \tag{2.22}$$

where n_2 is the nonlinear refractive index, neglecting absorption, A_{eff} is an effective mode area and ω_0 is the center frequency.[6] The second term on the left-hand side of equation 2.21 shows how pulses tend to spread due to group velocity dispersion, and that the term on the right-hand side shows how pulses tend to spread due to self-phase modulation (see section 2.4.1).

[6] It is possible to include higher order dispersion terms as well as the Raman effect into a similar propagation equation. This is beyond the scope of this report

2.4.4. Solitons

It is possible for the effects of group velocity dispersion to compensate for the nonlinear effect (of self-phase modulation) if the group velocity dispersion is negative. Under appropriate conditions an optical pulse can indeed propagate through a dispersive, nonlinear medium with an invariant shape. Such pulses are known as optical solitons. A solution to equation 2.21 whose shape does not change is ([14], p. 281)

$$A(z,\tau) = A_0 \text{sech}\frac{\tau}{\tau_0} \exp\left(i\frac{-\beta_2}{2\tau_0^2}z\right) \tag{2.23}$$

where the soliton pulse amplitude A_0 and the soliton pulse width τ_0 must be related according to

$$|A_0|^2 = \frac{-\beta_2}{\gamma\tau_0^2} \tag{2.24}$$

β_2 and γ must have opposite signs to represent a physical pulse. Because γ is always ≥ 0, optical solitons can only exist in the anomalous dispersion regime ($\beta_2 < 0$).

Soliton Self-Frequency Shift

In the derivation of the NLSE the response of the medium was assumed to be instantaneous. However, the contributions to the nonlinearity from molecular vibrations (optical phonons) is non-instantaneous and gives rise to the Raman effect. The Raman effect leads to a gain of the red frequency components relative to the blue frequency components of the pulse. This results in a red-shift of the whole pulse and is known as the soliton self-frequency shift. The red-shift is strongest for the highest order soliton (corresponding to the shortest pulse). This Raman-induced frequency shift can be written as ([11], p. 186)

$$\Delta\omega_R(L) = \frac{-8|\beta_2|T_R L}{15\tau_0^4} \tag{2.25}$$

where T_R is a characteristic response time for the Raman gain, and τ_0 is again the soliton width. Note that the frequency shift scales with β_2 and fiber length L. To numerically calculate the Raman effect on spectra, the NLSE needs to be expanded [17] [18].

Coupling to Dispersive Waves

Non solitonic radiation (NSR) can be emitted if a normal dispersive wave is phase-matched to a soliton via a four wave mixing process. The condition for this to happen is when $\Delta\phi = \phi_S - \phi_{NSR} = 0$. These phases of the soliton (S) and the dispersive wave (NSR) are given by [8]

$$\phi_S = \left(\beta(\omega_S) + \frac{n_2\omega_S|E|^2}{c}\right)L - \omega_S\frac{L}{v_{g,S}} \tag{2.26}$$

$$\phi_{NSR} = \beta(\omega_{NSR})L - \omega_S \frac{L}{v_{g,S}} \tag{2.27}$$

where $v_{g,S}$ is the group velocity of the soliton and L is the fiber length. The phase condition $\Delta\phi = 0$ leads to

$$\beta(\omega_S) + \frac{n_2\omega_S|E|^2}{c} - \beta(\omega_{NSR}) = 0 \tag{2.28}$$

and is actually independent of fiber length and group velocity. In principle this allows us to predict in which part of the spectrum the NSR light will be generated.

3. Experimental Setup

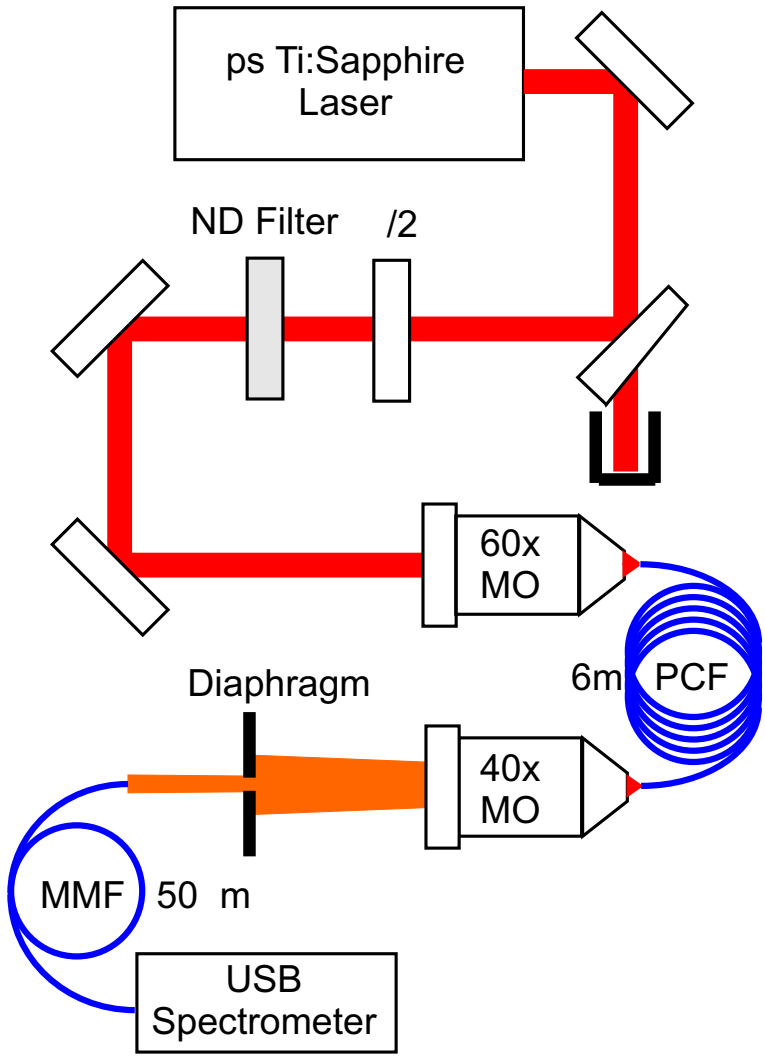

Figure 6: Schematic of the experimental setup.

The experimental setup used to generate a supercontinuum is shown in figure 6. It consists of three parts. In section 3.1, we describe the PCF in which the supercontinuum is generated. Section 3.2 describes the pump laser and the optics used to couple the pump into the fiber. Section 3.3 finally describes the collection setup which is used to collect and analyze the generated spectra.

3.1. Fiber Parameters

The single-mode step-index photonic crystal fiber used is the NL-PM-750 with a fiber length of 6 m, manufactured by Crystal Fibre. It has the following properties [4]:

- two zero-dispersion wavelengths, one at 750 ± 15 nm and one at 1260 ± 20 nm (see section 2.3).
- an effective core diameter of $1.6 \pm 0.3\,\mu$m at 780 nm, related to the effective core area.
- a nonlinear coefficient of $\gamma = \sim 95\ (\mathrm{Wkm})^{-1}$ at 780 nm (see sections 2.4.1 and 2.4.3).
- a cutoff wavelength $\lambda_c \leq 650$ nm for multi-mode operation (see section 2.1)
- a numerical aperture of 0.38 ± 0.05 at 780 nm.
- an attenuation < 0.05 dB/m at 780 nm
- a birefringence of $\Delta n > 3{\cdot}10^{-4}$ (see section 2.1).

3.2. Pump Setup

The PCF is pumped by a picosecond mode-locked Ti:sapphire laser,[7] pumped by a 7 W 532 nm CW diode laser.[8] The wavelength can be tuned in the range between 700 and 1000 nm, while the average power varies from 250 mW at 1050 nm to 1.5 W at 790 nm ([15], p. 3-13). The laser has a repetition rate of 82 MHz, a beam diameter of $\sim$2 mm and the laser output is linearly polarized.

The average laser power of $\sim$1 W was reduced to $\sim$100 mW by reflecting the beam on a glass wedge under a 45^o angle. The intensity was further controlled by a set of neutral density (ND) filters. The polarization of the input beam is controlled with a $\lambda/2$ waveplate. The pump beam is coupled into the fiber using a 60x microscope objective[9] (60x MO) on a XYZ stage. The 60x MO has an anti-reflection coating for visible wavelengths and reflects a certain amount of light for wavelengths above 800 nm. These back reflections can interfere with mode-locking inside the laser cavity. This is avoided by slightly misaligning the beam and using filters to reduce the reflections (at 836 nm in particular).

The average power coupled into the fiber (ACP) is determined by measuring the optical power at the output facet of the fiber with a thermal photodetector. The measured power typically has a standard deviation of $\sim$0.2 mW. A coupling efficiency η - defined as ACP/input power - as high as 50% could be achieved. After a pump wavelength is selected the spectrum of the laser is measured to determine this wavelength within 0.2 nm accuracy. A stable pulse is found and the auto-correlator function is measured to get the pulse width within 0.1 ps accuracy. The beam is aligned such that the coupling

[7] Spectra Physics Tsunami
[8] Spectra Physics Millenia X
[9] Newport M-60X, NA = 0.85, f = 2.9 mm

efficiency is at least 30%.

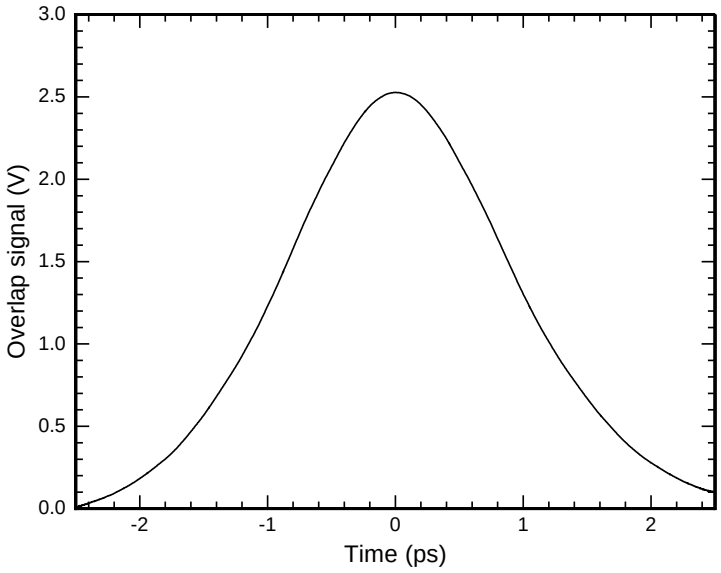

Figure 7: Auto-correlation function of a typical laser pulse. The time axis has been obtained by the relation given in equation 3.1.

The pulse width of the laser pulse was measured using an auto-correlator setup. In this setup, the auto-correlator overlaps the pulse signal with a copy of itself inside a BBO crystal using a conventional interferometer setup, where second harmonic light is generated proportional to the measure of overlap. This overlap function can be described as a convolution integral of two signals, see ([10], pp. 539-543). Figure 7 gives a typical auto-correlation function (acf). The FWHM of this acf is 2.0 ps.

The acf has been recorded on a digital oscilloscope using one of the outputs of the auto-correlator. This output monitors the second harmonic intensity while the auto-correlator moves one of its interferometer arms at a scanrate of 16,7 Hz in a sinusoidal motion over a distance expressed as the scanrange. The scanrange is 5 ps in this case which corresponds to a distance of 1.5 mm; the amplitude x_0 is then 0.75 mm.

The position of the interferometer arm as a function of time is given by: $x_{acf} = x_0 \sin(2\pi f t_{acf})$. At the same time we also know the distance travelled by the pulse which is the pulse time multiplied by the speed of light: $x_{pulse} = ct_{pulse}$. The two time scales are related by

$$t_{pulse} = \frac{x_0}{c} \sin(2\pi f t_{acf}) \tag{3.1}$$

The auto correlation function typically looks Gaussian, but the shape of the original pulse is lost. You cannot deconvolute and hope to get it back, unless you have additional information about your original pulse composition (in particular, phase information is lost).

3.3. Collection and Analysis Setup

The generated supercontinuum is collected using a 40x MO[10] at the exit of the fiber and a small fraction ($\sim(50\,\mu\text{m}/25\,\text{mm})^2 \approx 2{\cdot}10^{-6}$) using a pinhole is collected by a 50 μm core multimode fiber (MMF) and sent to a spectrometer. All spectra are taken using SpectraSuite software provided by Ocean Optics. The results are measured using 3 different spectrometers (the USB4000, USB2000 and the NIR512) to cover the visible and infrared range.

The spectrometers use a grating and spread the light of different wavelengths out over an array. This array is a linear silicon CCD array for the USB4000 and the USB2000 and a InGaAs array for the NIR512. These detectors have a saturation level (related to the pixel well depth of the array) which they were prevented from reaching by setting the integration time by software. Spectra taken by the same spectrometer, but with different integration times, are corrected for this difference so they can be compared directly.

The wavelength resolution for data from USB4000 spectrum analyzer varies from 0.22 nm to 0.17 nm for wavelengths from respectively 178.14 nm to 886.96 nm (average 0.195 nm). For the USB2000 resolution varies from 0.38 nm to 0.26 nm for wavelengths from respectively 519.87 nm to 1172.85 nm (average 0.32 nm). For the NIR512 resolution varies from 1.72 nm to 1.67 nm for wavelengths from respectively 854.65 nm to 1722.32 nm (average 1.695 nm).

To correct our spectra for the response of the detector and the grating, we measured the spectrum of a tungsten calibration lamp at a temperature of 3200 K. The spectrometers generate spectra that are compared to a black body radiation curve that is given by

$$u(\lambda, T) = \frac{8\pi hc}{\lambda^5} \frac{1}{\exp(\frac{hc}{\lambda kT}) - 1} \tag{3.2}$$

for T = 3200 K. The result is given in figure 8. The response of each detector is obtained by dividing the measured spectrum by the black body radiation spectrum, and normalized such that the highest response equals 1. The normalized responses are shown in figure 9. All measured supercontinuum spectra are divided by the response function of their spectrometers to obtain intensity-calibrated spectra.

[10] Newport M-40X, NA = 0.65, f = 4.5 mm.

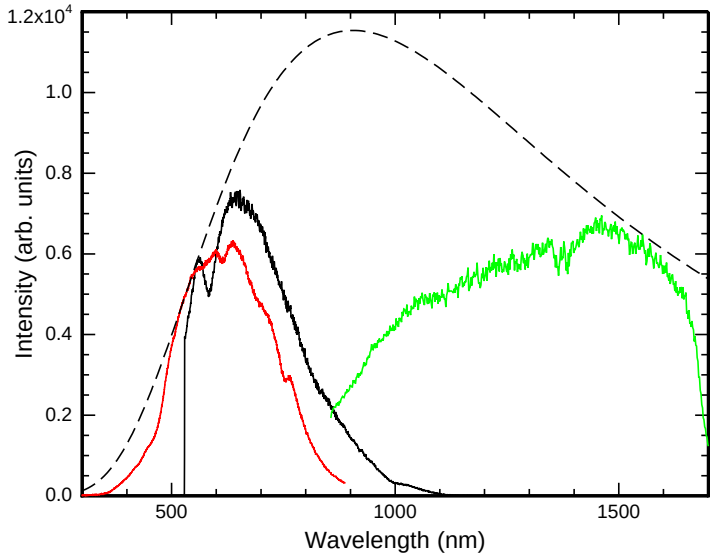

Figure 8: White light calibration spectra. The graphs are measured responses from the USB4000 (red), USB2000 (black) and the NIR512 (green) spectrometers. The dashed line is the black body radiation spectrum for T = 3200 K.

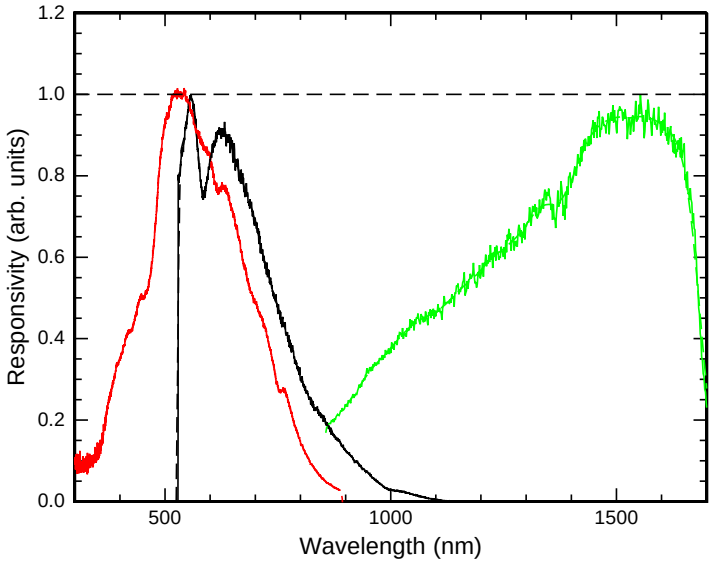

Figure 9: Responsivity of each detector. The graphs are measured responses from the USB4000 (red), USB2000 (black) and the NIR512 (green) spectrometers.

4. Results

We start with the polarization dependence of the measured spectra in section 4.1, and check the influence of the birefringence on white light spectra. The pump wavelength dependence is covered in section 4.2, to identify different regimes of dispersion. Finally, in section 4.3 the details of supercontinuum generation are studied by investigating the power dependence at a constant pump wavelength.

4.1. Polarization Dependence

Figure 10 shows a typical white light spectrum generated by the PCF using pump wavelength 754 nm (vertical red line), pulse duration 2.0 ps and 32.6 mW ACP. The vertical red line indicates the pump wavelength. Clearly, the highest peak in the spectrum corresponds to the pump. A broadband spectrum extends to the blue and the red with well defined edges, especially on the blue side around 530 nm. The measurement in figure 10 was done with the $\lambda/2$ plate set at 20°.

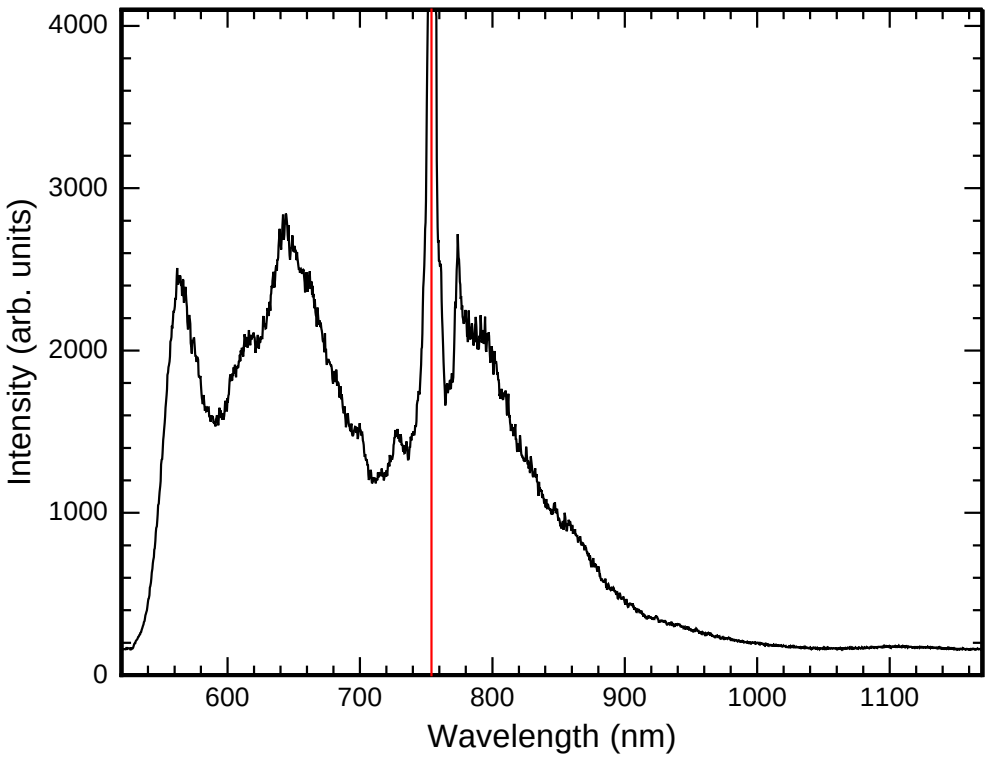

Figure 10: Typical white light spectrum generated at pump wavelength 754 nm (vertical red line), pulse duration 2.0 ps and 32.6 mW ACP. This spectrum is not corrected for the detector response.

To test and show the polarization-maintaining characteristic of our fiber, the polariza-

tion was changed over 180° by changing the $\lambda/2$ plate over 90° in steps of 2°. In figure 11 a (polar) density plot of the measured spectra between 520 nm and 620 nm is shown as a function of the angle of the $\lambda/2$ plate. The angle over which the linear polarization is rotated is twice the angle of the $\lambda/2$ plate. The wavelength is plotted from 520 nm to 620 nm, to clearly show that the edge of the spectrum is shifted depending on the input polarization. The blue edge varies between 529 nm and 564 nm. Between 800 nm and 1000 nm a similar plot can be made (not shown), but the sinusoidal form is disrupted by background noise.

When the $\lambda/2$ plate is at 20°, i.e. the polarization is rotated over 40°, the measured spectrum is blue shifted the most. When the $\lambda/2$ plate is at 65° and the polarization is rotated by 90° to 130°, the spectrum is red shifted the most. The sinusoidal shape as observed in figure 11 suggests that the polarization dependence of our fiber is relatively simple.

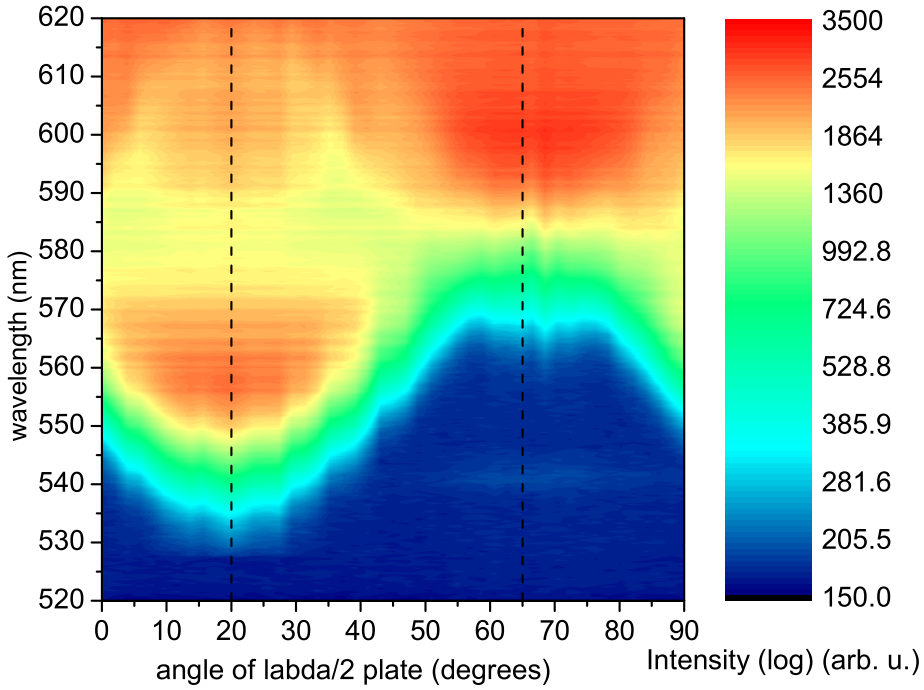

Figure 11: Polarization measurement, density plot; pump wavelength 754 nm, ACP 32.6 mW, pulse width 2.0 ps. The fast axis is at 20^o $\lambda/2$ plate, the slow axis is at 65° $\lambda/2$ plate, indicated by the dashed lines. These spectra are not calibrated or normalized.

4.2. Wavelength Dependence

By varying the wavelength around the zero order dispersion wavelengths one would expect to observe qualitative changes in the measured spectra. In figure 12, the pump wavelength is varied and 3 different characteristic spectra were taken between 738 nm and 850 nm. In the wavelength area between 758 nm and 768 nm, water and oxygen vapor prevented a stable operation of the laser ([15], p.3-11). Below a pump wavelength of 738 nm, no significant spectral broadening was witnessed, despite sufficient ACP and a stable pulse. Clearly $\beta_2 > 0$ there.

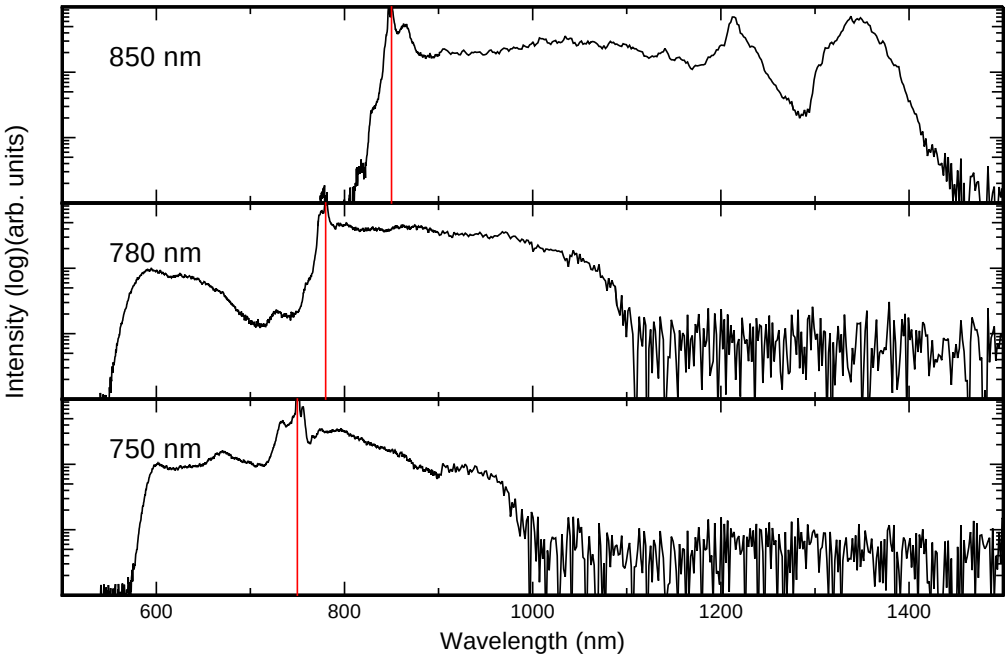

Figure 12: Wavelength measurement, logarithmic scale; polarization 0° (not the slow/fast axis), ACP 24 mW, pulse width 2.5 ps. Characteristic spectra for pump wavelengths at 750, 780 and 850 nm are shown.

Though the range of the different spectra increases with pump wavelength, spectra at 738, 742, 746, 750, 754 and 758 nm show a similar broadband shape to the one given (750 nm). Spectra at 770, 775 and 780 nm have a clearly different, less symmetric shape. The intensity drops an order of magnitude on the blue side of the pump. This is clearly visible in figure 12 for a pump wavelength of 780 nm in the spectral region between 700 and 750 nm. At 850 nm, the generation of wavelengths on the blue side of the pump is more than 2 orders of magnitude less and the spectrum mostly extends to the red side of the pump. This suggests that the spectrum at 780 nm represents a mix between the spectrum at 750 nm and the spectrum at 850 nm.

From these results it seems reasonable to classify supercontinuum generation for dif-

ferent pump wavelengths into two different regions, based on the dispersion curve:

- **zero-dispersion**, or close to it, $\beta_2 \approx 0$. Spectra with a pump wavelength of between 738 and 758 nm fall in this category. The generated spectra are more or less symmetric and extend to the blue and the red of the pump wavelength.
- **anomalous dispersion**, $\beta_2 < 0$. The generated spectra are strongly asymmetric and extend more to the red side of the pump than to the blue side. Spectra with a pump wavelength of 770 and higher exhibit this behavior.

Figure 13 shows all measurements between 738 and 780 nm in a density plot. The false color plot was obtained via interpolation of the measured spectra. The pump wavelengths at which measurements were done are indicated by the dashed vertical lines. In figure 13 it is clearly seen that the supercontinua gradually change for increasing pump wavelength. The spectra become broader, i.e. they extend more to the red as well as to the blue. For pump wavelengths beyond 770 nm the spectra become strongly asymmetric as is witnessed by the blue area in the lower right corner of figure 13.

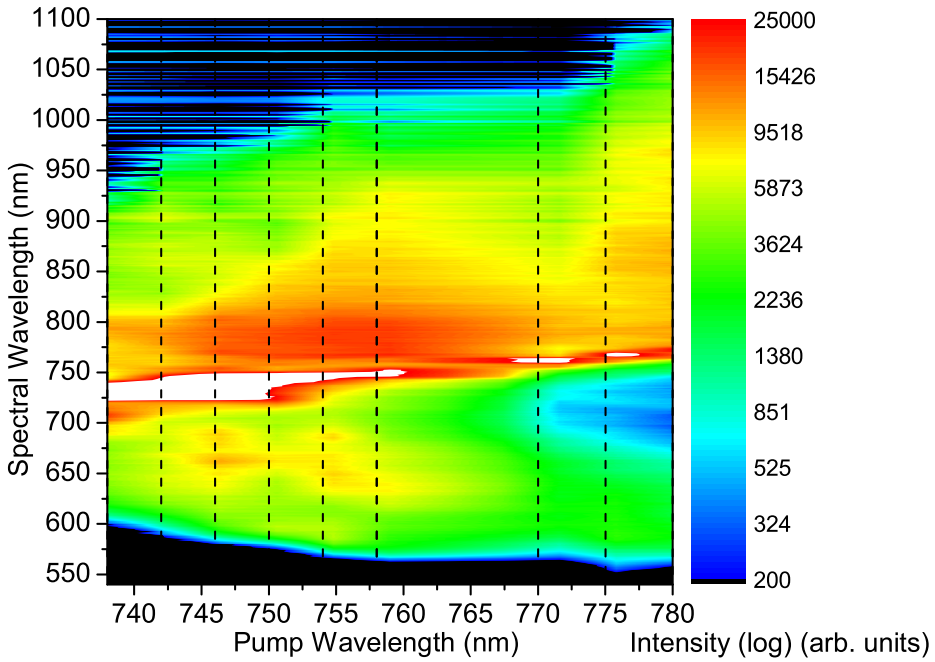

Figure 13: Wavelength measurement, logarithmic scale, density plot; polarization 0° (not the slow/fast axis), ACP 24 mW, pulse width 2.5 ps. 9 measurements were made at 738, 742, 746, 750, 754, 758, 770, 775 and 780 nm, represented by the dashed vertical lines.

Wavelength dependence on the blue side of the pump in the anomalous dispersion regime

In the anomalous dispersion regime and at low power, a single peak is visible on the blue side of the pump wavelength. We varied the pump wavelength and recorded the peak position without taking particular care of the exact ACP and pulse width. The measurements were made at a reduced ACP where the blue spectral sideband starts to grow and are shown in figure 14. The spectra have been normalized to the peak intensity of the blue spectral sideband. Since the absolute value of the peak intensity varies, the noise differs for the different spectra. For all wavelengths a relatively weak peak is detected that shifts with pump wavelength. The red part of the spectrum is not measured and assumed to have a higher intensity than the blue peaks. We observe a small shift of these peaks to the blue with increasing pump power. The spectra in figure 14 correspond to the lowest possible pump power and the longest possible peak wavelength.

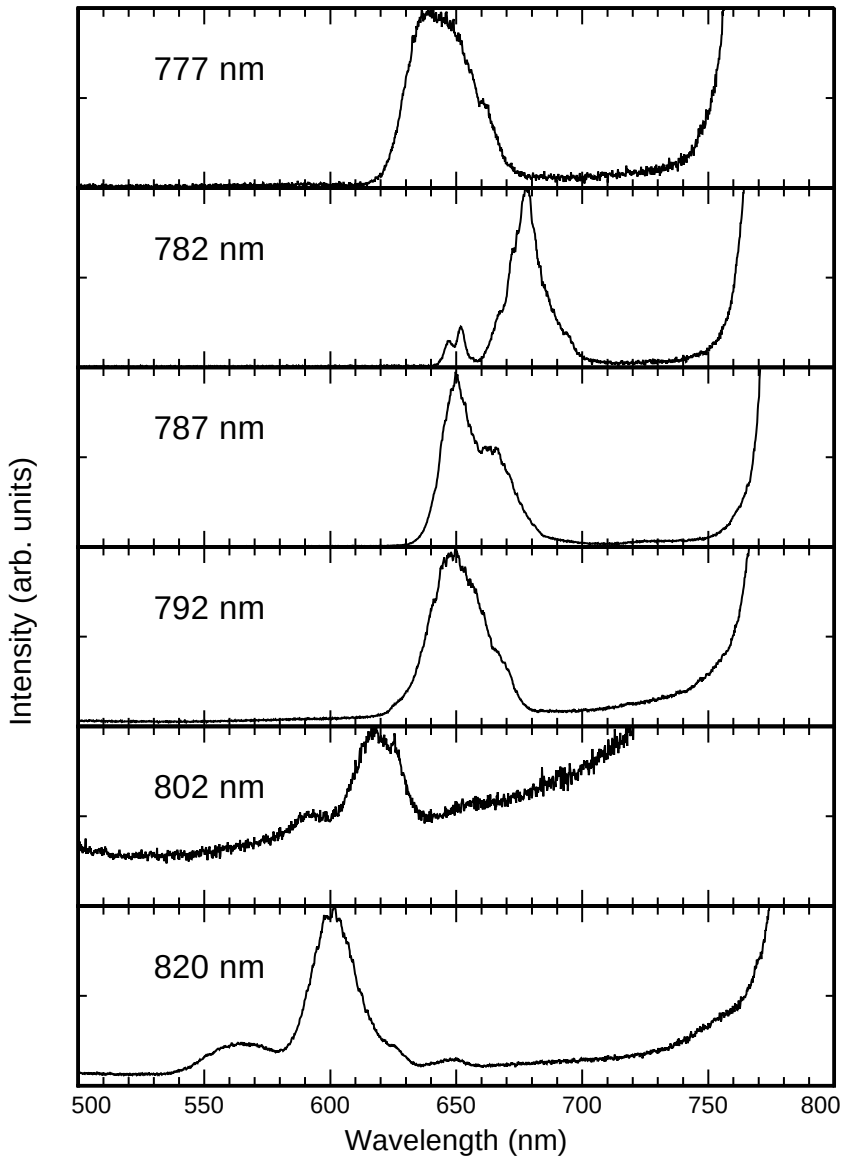

Figure 14: Wavelength measurement, following the light generated on the blue side of the pump; Polarization = 130° (slow axis). ACP and pulse width vary. These spectra are each normalized to 1, noise levels may vary.

4.3. Power Dependence

In this section we study the influence of the average coupled power (ACP) on the generated supercontinuum spectra in both the zero-dispersion and anomalous dispersion regimes. Decreasing ACP to below a value between 1 to 2 mW typically gives a spectrum with a single peak at the pump wavelength. By increasing the pump power (ACP), we can follow the supercontinuum generation and hopefully get some hints about the underlying nonlinear processes.

4.3.1. Zero-Dispersion Regime

Figures 15 and 16 show the measured supercontinua spectra as function of ACP for a pump wavelength of 738 and 754 nm. The value of the ACP for each spectrum is indicated by the label, more spectra have been recorded for intermediate values.[11] These spectra are not shown for clarity reasons, but follow the trend observed in figures 15 and 16.

The data in figures 15 and 16 show that the spectrum gradually broadens for increasing pump power. For a pump wavelength of 738 nm (figure 15) a clear peak is observed on the blue side of the pump. This peak is clearly visible for intermediate pump powers and shifts to the blue side for increasing pump power. At high level pump power ($>$ 17 mW) this feature broadens and results in a more or less flat spectrum on the blue side of the pump.

The data in figure 16 show that at a pump wavelength of 754 nm the generated spectra are more symmetric, especially for high pump powers. Although the pump power and pulse duration are very similar, the conversion of the pump is much more efficient at 754 nm. This is easily seen by the fact that the pump peak almost disappears at the highest pump power (32.6 mW) in figure 16, while it is still very present in figure 15 for the highest pump power (30 mW).

[11] 11 spectra were measured at $\lambda_p = 738$ nm for an ACP of 1, 3.5, 7.5, 9, 10.5, 14, 17, 22, 24, 26.5 and 30 mW. 15 spectra were measured at $\lambda_p = 754$ nm for an ACP of 1.55, 1.93, 2.63, 2.77, 4.00, 5.19, 6.14, 7.46, 10.1, 10.8, 14.0, 17.0, 22.8, 30.2 and 32.6 mW.

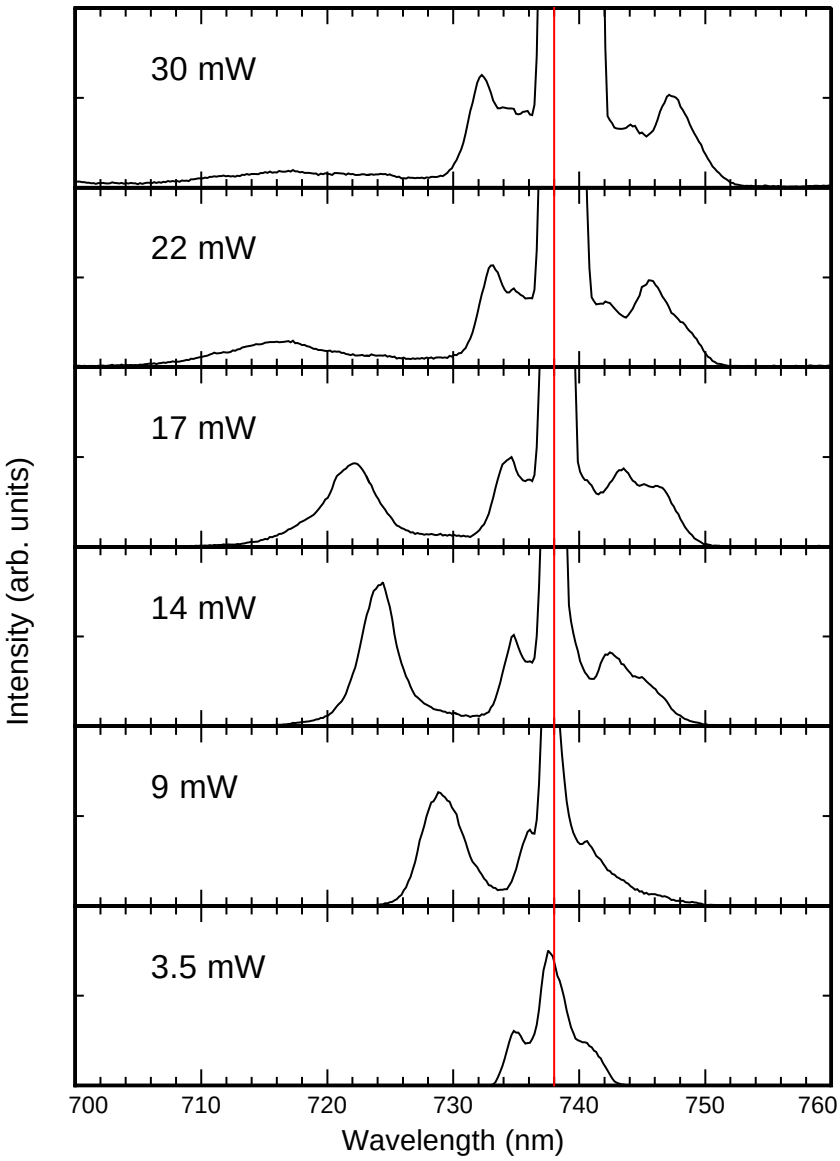

Figure 15: ACP measurement; pump wavelength 738 nm, pulse width 2.0 ps. The ACP is indicated by the labels in the figure. Note the asymmetric side peak generation starting at 9 mW.

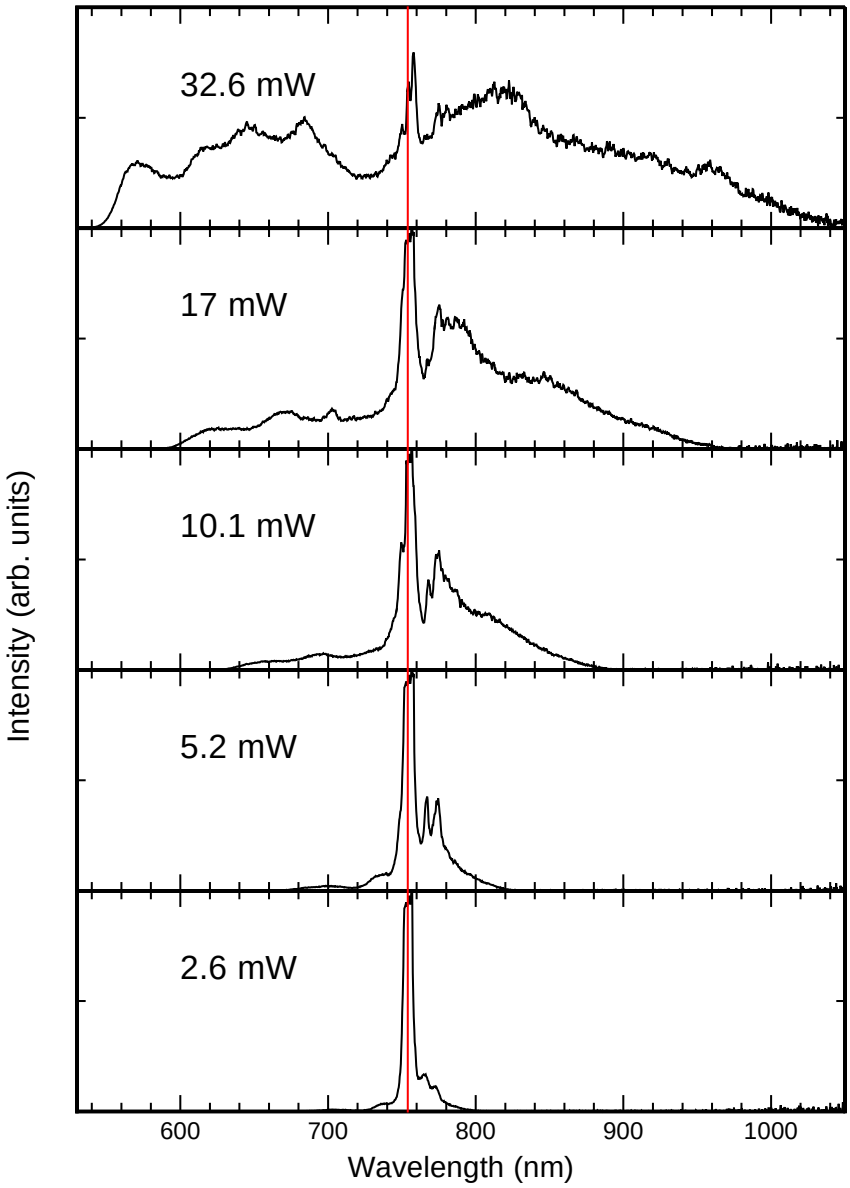

Figure 16: ACP measurement; pump wavelength 754 nm, pulse 2.0 ps. The ACP is indicated by the labels in the figure. On the red side of the pump intensities are higher than on the blue side, for an ACP up to 22 mW. At the highest ACP the spectrum becomes more symmetric.

4.3.2. Anomalous Dispersion Regime

Figure 17 shows the measured power dependence in the anomalous regime at a pump wavelength of 836 nm (figure 17). The asymmetry of the spectra is striking. No supercontinuum was generated at the blue side of the pump for pump powers up to 12 mW. Higher pump powers are not possible at this pump wavelength because reflections from the microscope objective disturb the mode-locked operation of the laser (see section 3.2).

Especially at the lower pump powers a clear Gaussian shaped peak is visible at the red side of the pump. The peak continuously shifts to the red with increasing pump power. The frequency shift with increasing ACP as observed in figure 17 can be quantified. For the first four spectra (up to 7.10 mW) the peak position of the longest wavelength peak is noted. For higher ACP, a gaussian shape is loosely drawn through the longest wavelength peak and its center position (λ_S) is noted.

Figure 18 shows the frequency shift $\Delta\omega^2 = (\omega_S - \omega p)^2$ as a function of ACP. Note that we plot the square of the frequency shift. A straight line in figure 18 thus gives a shift that increases linearly with the field amplitude (given by the square root of the ACP). Our experimental data is best described by such a dependence and the best fit to the data (red line in figure 18) gives a slope of 1.33 $\pm$ 0.05 $10^{28}\mathrm{Hz}^2\mathrm{mW}^{-1}$ and an offset of -3.64 $\pm$ 0.38 10^{28} Hz^2. This offset on the vertical axis corresponds to an ACP of 2.74 $\pm$ 0.27 mW below which no shift is observed, called a threshold. Similar linear relations have been found for pump wavelengths at 850 nm and 754 nm. For those wavelengths there are fewer data points at low pump powers and it is more difficult to establish a threshold as observed in figure 18.

At 850 nm we were able to reach larger values of ACP. The recorded spectra resemble those for 836 nm pump wavelength and are strongly asymmetric. The spectrum for an ACP of 24 mW is shown in figure 12 (top) and extends to $\sim$1400 nm. Spectra for an ACP of 21.3 and 36.4 mW are shown in figure 19 over a wavelength range from 500 to 1500 nm. For these values of the pump power the spectrum does not extend further to the red beyond 1400 nm; the red sideband peaks around 1215 and 1345 nm do not shift with increasing pump power. The structure in the spectral range between the pump (850 nm) and the first peak (1215 nm) do change with increasing ACP. A clear dip in the intensity is visible in between the two peaks around 1285 nm.

Close inspection of the blue side of the spectrum reveals a small peaks around $\sim$550 nm and $\sim$780 nm. These blue sideband peaks are shown in more detail in figure 20 for different values of the ACP. Additional measurements were done at an ACP of 24.1, 29.1, 33.0 and 35.4 mW (not shown). The peaks grow in intensity with increasing ACP, but do not shift. At these high pump powers, the fiber lights up more or less uniformly with a green to yellow color.

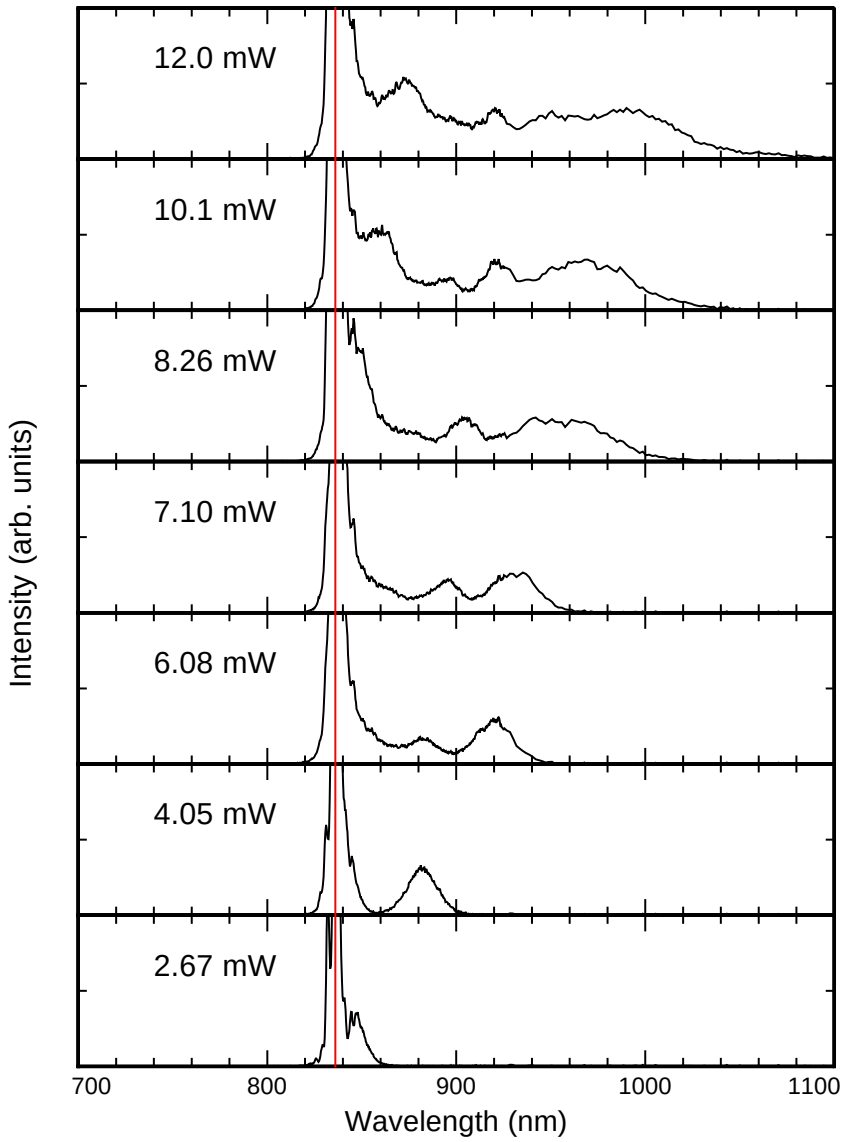

Figure 17: ACP measurement; polarization 40°, pump wavelength 836 nm, pulse width 3.5 ps. The ACP is indicated by the labels in the figure.

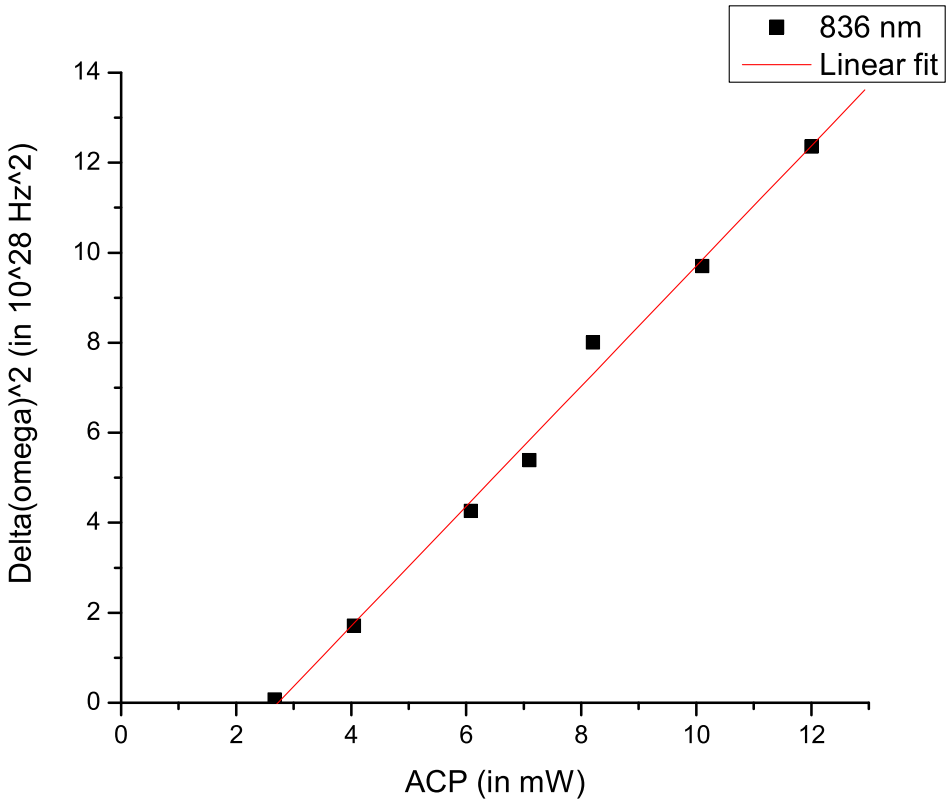

Figure 18: Shift of the leading peak (center frequency ω_S) in figure 17. The frequency shift is expressed relative to the pump frequency ω_p as a function of ACP.

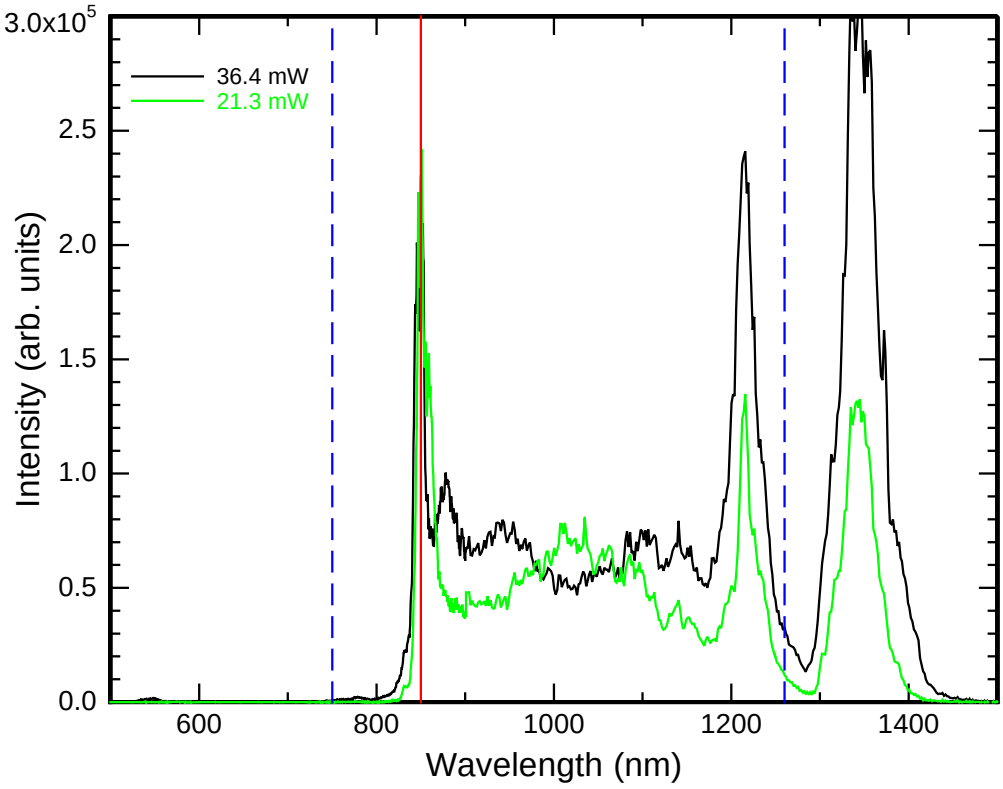

Figure 19: ACP measurement for an ACP of 21.3 mW and 36.4 mW; polarization 40°, pump wavelength 850 nm, pulse width 2.5 ps. The ACP is indicated by the labels in the figure. The dashed blue lines indicate the position of the zero-dispersion wavelengths.

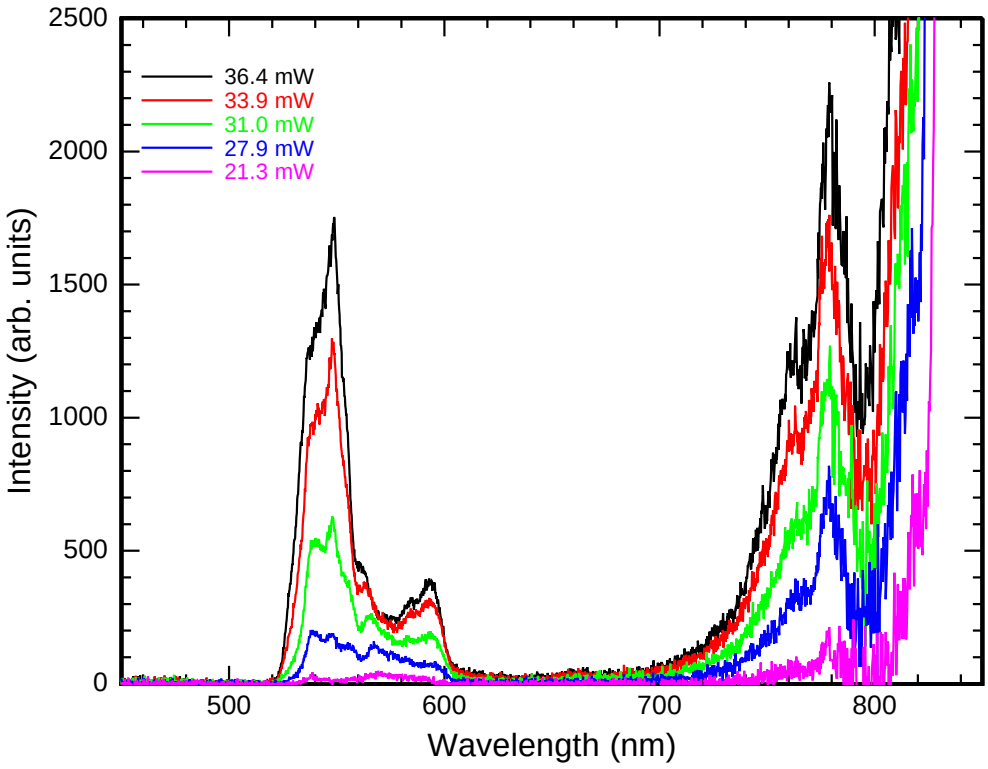

Figure 20: ACP measurement on the blue side of the pump wavelength in the anomalous dispersion regime; polarization 40°, pump wavelength 850 nm, pulse width 2.5 ps. The ACP is indicated by the labels in the figure.

5. Discussion

In this section the results will be compared to two simplified pictures. The first picture is based on four wave mixing (section 2.4.2) and assumes that FWM is the main mechanism to generate broadband continua. The second is based on solitons (section 2.4.4), their subsequent Raman-induced frequency shifting and coupling to dispersive waves for generating new spectral components.

- **Four wave mixing model**. Shorter and longer wavelengths are generated by direct FWM of 2 pump photons. The phase-matching condition requires the dispersion to be negative at the pump frequency. For increasing ACP the generated spectrum range broadens due to the nonlinear contribution (γP_0) to the phase-matching condition. The signal and idler frequencies should be growing towards the pump for increasing ACP (see figures 4 and 5) [3] [2].
- **soliton model**. For sufficiently high pump power, solitons can be formed when the pump wavelength is in the anomalous dispersion regime. Frequencies on the red side of the pump can be generated by self-frequency shifting of solitons due to the Raman effect. This shift becomes stronger for higher ACP, leading to broader spectra on the red side of the pump. Frequencies on the blue side of the pump can be generated by solitons coupling to dispersive waves. Increasing ACP does not change their spectral position as they do not depend on pump wavelength but only on the soliton generating them [16] [8].

5.1. Results Obtained with a FWM Model

We will first compare the four wave mixing simulation results with our measurements. The measured spectra in the density plot of figure 13 are too broad to be directly explained by the phase-matching curves calculated in section 2.4.2. From figure 5, it is evident that the four wave mixing model can never give spectral components below 520 and above 1910 nm. For pump wavelengths near the zero order dispersion wavelengths, a large number of phase-matched wavelengths appear (see figure 5), validating almost any spectrum measured there.

Moving the pump wavelength into the anomalous regime and setting the ACP to a low value should generate the the most outlying curve in figure 5. The measured frequencies of these small peaks are presented in figure 14. The peak positions of the blue sideband are plotted together with our most accurate phase-matching curve (using a 6th order polynomial approximation) in figure 21. The green data points correspond to an input polarization of 40°; the blue data points correspond to a 130° polarization. The red dots indicate the calculated phase-matching curves using FWM for 3 different values of γP_0. The most outlying curve corresponds to $\gamma P_0 = 0$. The linear line in the top left corner corresponds to the trivial solution $\lambda_p = \lambda_s = \lambda_i$.

What we find is a complete mismatch with experiment. The measured points do not follow the outlying theoretical curve (red dots in figure 21, $\gamma P_0 = 0$). Additional phase-matching curves have been calculated for $\gamma P_0 \neq 0$, but the measured data clearly do not follow the predicted trend. According to all phase-matching curves, the light generated at shorter wavelengths should move towards longer wavelengths as the pump wavelength increases. Instead, it moves towards shorter wavelengths.

Another interesting feature to note is the distinct peak on the blue side of the pump for an ACP between 9 and 17 mW in figure 15, seemingly without a longer wavelength counterpart. A similar asymmetry can be found in figure 16; the photons on the blue side do not have a clear counterpart in on the red side. To create one signal photons around 550 nm using two pump photons around 754 nm, one idler photon around 1200 nm should appear. Instead, no infrared photons are generated beyond 1050 nm.

These shortcomings in both the anomalous and zero-dispersion regime show that the simple four wave mixing hypothesis as suggested in [3] for generating new spectral components the picosecond regime is questionable.

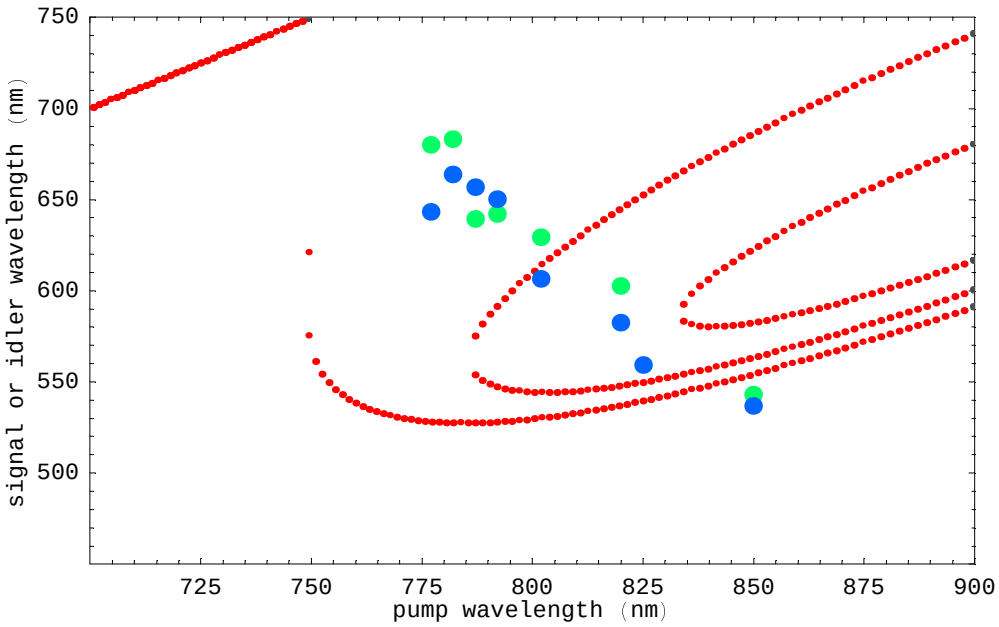

Figure 21: Comparison of the four wave mixing model (red dots) with experimental data (green and blue points). The green and blue points indicate measured frequencies (data taken from figure 14) of the blue sideband observed for the lowest ACP where they are still visible. The different theoretical curves correspond to phase-matching conditions with different values of γP_0.

5.2. Results Obtained with a Soliton Model

The soliton hypothesis finds its validation more through describing and understanding the generation of broadband spectra than through calculations, since solving the NLSE is difficult, lengthy and numerical. The frequency shift observed in figure 17 and the linear relation in figure 18 are consistent with observations and calculations made by others [17] [18].

A clear threshold is found in figure 18. The data in the anomalous regime (section 4.3.2) can be understood qualitatively as follows: Below a certain threshold power no solitons are formed and no frequency shifting occurs. Above the threshold a soliton forms. The Raman effect causes a frequency shift of the soliton that scales with the square root of the pump power [19] [16].

The relatively weak peaks on the blue side of the pump in figures 20 and 19 might be explained if the solitons couple to dispersive waves [8]. This coupling to dispersive waves does not depend on the wavelength of the pump but on the wavelength of the soliton generating them (see equation 2.28). If the soliton no longer frequency shifts because it reaches the second zero-dispersion wavelength, the phase-matching condition to create the dispersive waves would not change. This would explain why the peaks on the blue and red sides do not shift with pump power.

The intensity of wavelengths generated on the blue side of the pump decreases two orders of magnitude as the pump wavelength is moved into the anomalous dispersion regime (see figure 12) from 750 to 850 nm. This corresponds to a decrease of β_2 equal to -180 fs^2cm^{-1}. Apparently, the generation of blue light is very inefficient when β_2 is strongly negative. When the wavelength of the pump is tuned towards lower values of $|\beta_2|$, the generation of blue light becomes more efficient. This might be explained by the phase-matching condition for the coupling of dispersive wave to the soliton (equation 2.28). It would be desirable to evaluate this phase-matching condition in order to confirm that the blue light is indeed due to dispersive waves.

Close to the normal dispersion regime ($\beta_2 > 0$), a clear peak that shifts to the blue with increasing pump power is observed, see figure 15. Both the frequency shift as well as the Gaussian shape of the peak are remarkably similar to what is observed at a pump wavelength of 836 nm. The only difference being that the peak shifts to the blue and that it flattens out for higher pump powers. Clearly, the peak cannot be interpreted as a soliton, as solitons do not exist in the normal dispersion regime, nor do they flatten out (they split to lower-order solitons). We speculate that the peak on the blue side of the pump is still caused by dispersive waves from a soliton that exists in the anomalous dispersion regime. With increasing pump power, the phase-matching condition would change. Again, to quantitatively support this hypothesis a numerical solution of the phase-matching condition (equation 2.28) is necessary.

6. Conclusion

We have studied supercontinua generated with picosecond pulses in a 6 m long photonic crystal fiber (NL-750-PM, [4]). The supercontinuum that can be generated strongly depends on the pump wavelength and the peak power. We have varied the pump wavelength between 738 to 850 nm and the average coupled power (ACP) between 2 to 32 mW. No supercontinuum can be generated for pump wavelengths below 738 nm. Between 738 and 758 nm supercontinua are found that extend to the blue as well as to the red side of the pump. For pump wavelengths of 770 nm and longer, the measured spectra extend mostly to the red.

Our measured cannot be explained by a simple four wave mixing model. The measured spectra lack the symmetry expected, especially when the pump wavelength is tuned to the anomalous dispersion regime. Even in the zero-dispersion regime, the predicted Stokes bands are found missing. Therefore we conclude that direct four wave mixing of the pump to create new wavelengths is not important.

Instead our measurements strongly suggest that solitons are responsible for the observed features in the spectra. For pump wavelengths around 850 nm, the spectra extend mostly to the red and show a frequency shift that is linear with the amplitude of the pulse. Qualitatively this can be understood in terms of a self-frequency shift of the solitons due to the Raman effect. Within the same model, blue spectral components can be generated by coupling of the soliton to dispersive waves. To get a good quantitative agreement and to confirm this hypothesis one is required to numerically solve the phase-matching condition for dispersive waves and/or the nonlinear Schrödinger equation.

Acknowledgement

I would like to thank the following people:

- Michiel de Dood for his excellent supervision, his useful advices and especially his patience when explaining things more than once.
- Eduard Driessen for his useful advices and particular experimental insight.
- The Quantum Optics and Information group for their support, all the discussions and conversations at the coffee table.

References

[1] Kim P. Hansen and René E. Kristiansen. "Supercontinuum Generation in Photonic Crystal Fibers", www.crystal-fibre.com

[2] Thomas V. Andersen et al. "Continuous-wave wavelength conversion in a photonic crystal fiber with two zero-dispersion wavelengths", Optics Express, 2004, vol. 12, no. 17, pp. 4113-4122.

[3] Karen Marie Hilligsøe, et al. "Supercontinuum generation in a photonic crystal fiber with two zero-dispersion wavelengths", Optics Express, 2004, vol. 12, no. 6, pp. 1045-1054.

[4] http://www.crystal-fibre.com/datasheets/NL-PM-750.pdf

[5] http://en.wikipedia.org/wiki/Self-phase_modulation

[6] Masanori Koshiba and Kunimasa Saitoh. "Applicability of classical optical fiber theories to holey fibers", Optics Letters, 2004, vol. 29, no. 15, pp. 1739-1741.

[7] Niels Asger Mortensen and Jacob Riis Folkenberg, "Modal cutoff and the V parameter in photonic crystal fibers", Optics Letters, 2003, vol. 28, no. 20, pp. 1879-1881.

[8] A. V. Husakou and J. Herrmann. "Supercontinuum generation of higher-order solitons by fission in photonic crystal fibers", Phys. Rev. Letters, 2001, vol. 87, no. 20, pp. 203901-1 to -3.

[9] http://www.tpub.com/neets/tm/109-4.htm

[10] Eugene Hecht, 1998. *Optics*, 3rd ed., Addison-Wesley, MA.

[11] Govind P. Agrawal, 2001. *Nonlinear Fiber Optics*, 3rd ed., Academic Press, CA.

[12] Allan W. Snyder and John D. Love, 1983. *Optical Waveguide Theory*, Kluwer Academic Publishers, Dordrecht, Netherlands.

[13] http://en.wikipedia.org/wiki/Self-phase_modulation

[14] Robert W. Boyd, 1992. *Nonlinear Optics*, Academic Press, CA.

[15] Spectra Physics, 2002. Tsunami, User's Manual.

[16] J. Herrmann, et al. "Experimental evidence for supercontinuum generation by fission of higher-order solitons in photonic fibers", Phys. Rev. Letters, 2002, vol. 88, no. 17, pp. 173901-1 to -4.

[17] M. G. Banaee and Jeff F. Young. "High-order soliton breakup and soliton self-frequency shifts in a microstructured optical fiber", J. Opt. Soc. Am. B, 2006, vol. 23, no. 7, pp. 1484-1489.

[18] J. K. Lucek and K. J. Blow. "Soliton self-frequency shift in telecommunications fiber", Phys. Rev. A, 1992, vol. 45, no. 9, pp. 6666-6674.

[19] P. K. A. Wai, et al. "Soliton at the zero-group-dispersion wavelength of a single-model fiber", Optics Letters, 1987, vol. 12, no. 8, pp. 628-630.

A. Tables

Table 1: Values taken from the dispersion curve in figure 2, used for fitting. Values for ω are calculated from λ.

λ (10^{-9} m)	ω (10^{15} Hz)	β_2 (10^{-25}s^{2}m^{-1})
600	3.141593	0.3855
650	2.899932	0.2264
700	2.692794	0.1132
750	2.513274	0
800	2.356194	-0.1038
850	2.217595	-0.1792
900	2.094395	-0.2547
950	1.984164	-0.3208
1000	1.884956	-0.3679
1050	1.795196	-0.3868
1100	1.713596	-0.3679
1150	1.639092	-0.3113
1200	1.570796	-0.1887
1250	1.507964	-0.3774
1300	1.449966	0.2169
1350	1.396263	0.500
1400	1.346397	0.8774
1450	1.299969	1.3208
1500	1.256637	1.8873
1526	1.235065	2.1604

Table 2: Fitting parameters for 2nd and 6th order polynomial fits to β_2 in section 2.4.2. ω should be entered in units of 10^{15} Hz to give β_2 in units of 10^{-25} s^{2}m^{-1}.

$a + b\omega + c\omega^2$	$a + b\omega + c\omega^2 + d\omega^3 + e\omega^4 + f\omega^5 + g\omega^6$
a = 8.59221	a = 238.319
b = -8.1057	b = -603.905
c = 1.8015	c = 633.827
	d = -353.61
	e = 110.627
	f = -18.3883
	g = 1.26783